ACS NANO

www.acsnano.org

ARTICLE

Piezoelectric Micro- and Nanostructured Fibers Fabricated from Thermoplastic Nanocomposites Using a Fiber Drawing Technique: Comparative Study and Potential Applications

Xin Lu,[†] Hang Qu,[‡] and Maksim Skorobogatiy*[,†,‡]

[†]Génie Métallurgique and [‡]Génie Physique, École Polytechnique de Montréal, Montréal, Québec H3T 1J4, Canada

Supporting Information

ABSTRACT: We report an all-polymer flexible piezoelectric fiber that uses both judiciously chosen geometry and advanced materials in order to enhance fiber piezoelectric response. The microstructured/nanostructured fiber features a soft hollow polycarbonate core surrounded by a spiral multilayer cladding consisting of alternating layers of piezoelectric nanocomposites (polyvinylidene enhanced with $BaTiO_3$, PZT, or CNT) and conductive polymer (carbon-filled polyethylene). The conductive polymer layers serve as two electrodes, and they also form two spatially offset electric connectors on the fiber surface designed for the ease of connectorization. Kilometer-long piezoelectric fibers of sub-millimeter diameters are thermally drawn from a macroscopic preform. The fibers exhibit high output voltage of up to 6 V under moderate bending, and they show excellent mechanical and electrical durability in a cyclic bend−release test. The micron/nanosize multilayer structure enhances in-fiber poling efficiency due to the small distance between the conducting electrodes sandwiching the piezoelectric composite layers. Additionally, the spiral structure greatly increases the active area of the piezoelectric composite, thus promoting higher voltage generation and resulting in 10−100 higher power generation efficiency over the existing piezoelectric cables. Finally, we weave the fabricated piezoelectric fibers into technical textiles and demonstrate their potential applications in power generation when used as a sound detector, smart car seat upholstery, or wearable materials.

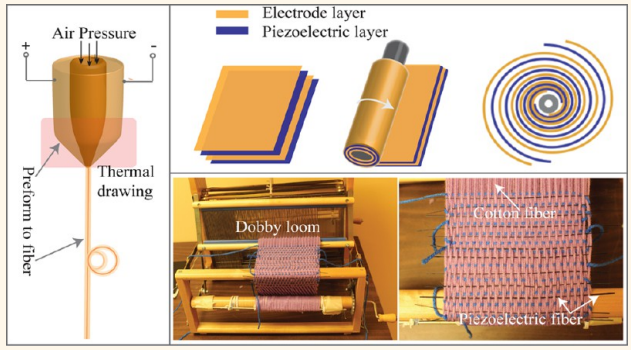

KEYWORDS: *flexible piezoelectric fibers, piezoelectric generators, energy-harvesting fibers, BTO−PVDF fibers, PZT−PVDF fibers, CNT−PVDF fibers, smart textiles, electronic textiles*

Over the past decade, significant effort has been put into the R&D of energy-harvesting and conversion devices that operate based on piezoelectric effect.[1−4] Unlike the energy harvesters utilizing solar or thermal energy, performance of piezoelectric generators is generally not limited by environment factors. An important driving force for developing piezoelectric energy generators is the growing popularity of personal wearable electronics such as on-garment displays, wearable sensors in sports and medicine, virtual reality devices, and smart watches and bracelets.[5−9] In these devices, piezoelectric generators or transducers utilizing mechanical energy from human body motions could be used as power sources or sensor components. Another emerging field where piezoelectric generators could find niche applications relates to self-energized electronics for automotive or aerospace industries. Piezoelectric generators harvesting energy from the traffic-induced vibrations or other parasitic mechanical movements could power on-board electronic systems such as wireless sensor networks (WSNs) with low-power consumption.[10,11] Note that, for these applications, piezoelectric generators in the form of fibers or strips are highly desired[12] because, due to their flexibility, they could be weaved seamlessly into multifunctional fabrics for wearable or on-board applications or, alternatively, coiled into compact energy generation cells.

Received: December 10, 2016
Accepted: February 3, 2017

DOI: 10.1021/acsnano.6b08290
ACS Nano XXXX, XXX, XXX−XXX

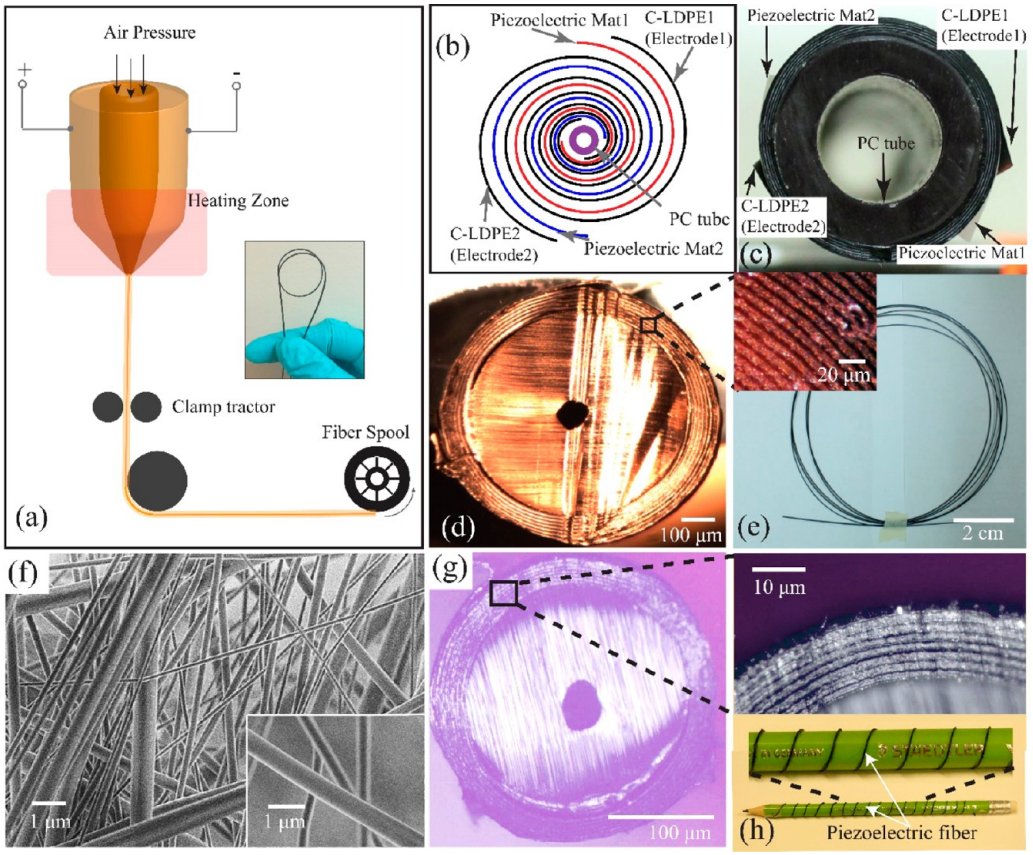

Figure 1. (a) Schematic of a fiber drawing process. (b) Schematic of the multilayer structure in the preform and in the drawn fiber. (c) Photo of a preform cross section. (d) Photo of a cross section of the piezoelectric fiber with a diameter of ~900 μm (drawn using 2 kV voltage on the preform electrodes). Inset: Magnified view of a multilayer structure. (e) Spool of a piezoelectric fiber. (f) Scanning electron microscopy images of the CNT/PVDF electrospun mats at different magnifications. (g) Photo of a cross section of the piezoelectric fiber with a diameter of ~300 μm (drawn using 5 kV voltage on the preform electrodes). Inset: Magnified view of a multilayer structure. (h) Piezoelectric fiber wrapped on a pencil.

Many attempts have been made to fabricate piezoelectric fibers. A simple method is directly depositing or wet-extruding ceramic piezoelectric materials such as ZnO nanowires (NWs), $BaTiO_3$ (BTO) NWs, and $Pb(Zr_{0.52}Ti_{0.48})O_3$ (PZT) NWs along a metallic wire/filament.[13−17] For instance, Qiu *et al.* reported a piezoelectric fiber fabricated by extruding a mixture of PNN−PZT powder and organic solvent along a Pt wire.[13] Wang and co-workers proposed a ZnO-based piezoelectric fiber fabricated by growing ZnO NWs on a Au-coated Kevlar fiber using a hydrothermal method.[14] Note that the mechanical reliability of these piezoelectric fibers could be problematic since frequent bending and surface abrasion would make the ceramic materials crack and even peel off from the fiber core. To improve robustness of the fibers, Wang and co-workers have proposed to cover the base of ZnO NWs with a protective polydimethylsiloxane (PDMS) layer using a method combining surface coating and plasma etching.[16] Instead of depositing piezoelectric layers onto a fiber/wire substrate, fabrication of piezoelectric fibers directly from piezoelectric polymers constitutes an alternative option. Compared to ceramic materials, piezoelectric polymers generally have better flexibility, thus they are more suitable for wearable applications. Among all of the piezoelectric polymers, poly(vinylidene fluoride) (PVDF) and poly(vinylidene fluoride-*co*-trifluoroethylene) (PVDF−TrFE) are predominantly utilized in piezoelectric devices due to the ease of thermal processing, high flexibility, high strain level, and good piezoelectric properties.[4]

Lund *et al.* used the melt-spinning method to fabricate a bicomponent fiber that had a PVDF sheath and a carbon-black-impregnated polyethylene (CB-PE) core serving as the inner electrode.[18,19] Using the same method, Roth *et al.* reported a piezoelectric fiber that had a PVDF sheath and carbon-nanotube-impregnated polypropylene (CNT-PP) core.[20] Recently, Liu *et al.* adopted an electrowetting-aided dry-spinning method to fabricate a piezoelectric fiber featuring a metallic core covered by a thin PVDF or PVDF−TrFE layer.[21] Piezoelectric fibers produced *via* the traditional spinning methods typically adopt a simple core−sheath structure, and the as-spun fibers may require an additional deposition of a metallic layer as an outer electrode that may have reliability issues due to surface abrasion and repeated bending or stretching actions. Also note that for PVDF piezoelectric fibers, high-voltage poling of the PVDF layers has to be performed during (or after) the spinning process in order to promote the nonpolar α to the ferroelectric β phase transition. In addition to electric poling of PVDF, one also uses stretching during the poling process, thus further complicating the fabrication process. PVDF−TrFE, on the other hand, could spontaneously crystallize into β phase during its solidification during a spinning process; however, compared to PVDF, the price of PVDF−TrFE is considerably higher.

Piezoelectric polymer fibers could also be fabricated using the fiber drawing technique. In this method, a geometrically complex multimaterial fiber preform with a length of tens of

DOI: 10.1021/acsnano.6b08290
ACS Nano XXXX, XXX, XXX−XXX

centimeters is first assembled using stacking of tubes, rods, multilayered films, or other functional components. Then, the preform could be drawn into fibers using a fiber drawing tower (Figure 1a). Geometry of the resultant fibers depends on parameters in the drawing process such as the temperature distribution in a furnace, the fiber drawing speed and the preform feed velocity, pressurization of the preform, as well as application of the electromagnetic fields. Fibers drawn from a macroscopic preform would generally retain the preform structure; however, sizes of the constituent elements will be reduced to micro- or even nanoscale. Therefore, various geometrically complex transverse structures that considerably enhance the fiber functionality could be realized within a fiber on a submicron scale by engineering the preform structure on a macroscopic scale and optimizing the conditions of the fiber drawing process. This, generally, cannot be accomplished by traditional fiber-spinning methods such as melt-spinning[22] or wet-spinning.[23,24] As an example, Egusa *et al.* demonstrated a multimaterial piezoelectric fiber using the fiber drawing technique.[25] This piezoelectric fiber featured a PVDF−TrFE piezoelectric layer sandwiched between two conductive polycarbonate (CPC) electrode layers and assembled with tin microfilaments for electrical connection. The fiber also had an outermost isolating PC layer serving as the protective cladding. An acoustic transducer was developed based on this fiber and showed a good response to acoustic waves with frequencies from kilohertz to megahertz. The fiber had several limitations, as it used very expensive PVDF−TrFE material, and it integrated in its structure a tin metallic microfilament, thus reducing the fiber reliability with respect to flexing. Finally, connecting to such fibers is challenging, as it requires manipulation with built-in micron-sized metallic electrodes. In ref 26, it was proposed that spontaneous piezoelectricity can be achieved in PVDF nanoribbons when using consecutive redrawings of the same fiber under high voltage. The authors claimed that under such conditions PVDF could crystallize into an exotic piezoelectric γ phase. At this point, it is difficult to evaluate the robustness of this fabrication technique, as there were no further reports of using this fabrication method. Additionally, multiple redrawing of the same fiber is needed for fabrication of PVDF nanoribbons, which could be labor-intensive and of low yield. To improve the piezoelectric properties of the drawn fiber, while avoiding using expensive PVDF−TrFE, a PVDF impregnated with ceramic piezoelectric materials such as BTO and PZT could be used instead.[27−29] Although a higher concentration of the ceramic fillers generally results in enhanced piezoelectric performance of PVDF, it would at the same time decrease the polymer viscosity,[25] thus eventually leading to capillary breakup of the fiber during drawing. Thus, the maximal concentration of ceramic fillers is limited by the drawing process. Furthermore, the CNT could also be impregnated into PVDF in order to enhance its piezoelectric properties *via* spontaneous formation of the β phase crystals in PVDF.[30−32] Incorporation of a small amount of CNT can lead to remarkable improvements of the electrical and mechanical properties of the PVDF fibers, as reported in ref 33. There, the authors argued that application of a shear stress to the polymer melt leads to the preferred orientation of the macromolecules, thus reducing the entropy of the polymer melt and leading to the flow-induced crystallization from the melt. Moreover, incorporation of the CNT can promote the shear-induced crystallization behavior and enhance the formation of β-crystals in PVDF nanocomposites. Also, the CNT could induce charge accumulation at the interface during an electrical poling process, thus further promoting the conversion of the PVDF molecules' α phase into the β phase.[30,31,34,35] Similar to the case of ceramic fillers, the maximum concentration of the CNT is also limited by the fiber drawing process.

In this paper, we report fabrication of the multimaterial piezoelectric fibers from perovskite ceramic nanoparticles (BTO/PZT)−PVDF and CNT−PVDF composites *via* fiber drawing. Furthermore, we perform a comparative study of the piezoelectric performance of the fabricated fibers. The proposed fibers feature a spiral geometry that significantly increases the fiber piezoelectric response. Due to the judicious arrangement of the conductive layers, connecting to our fibers is easy as the two electrodes occupy the opposite sides of the exposed fiber surface. The use of conductive plastic composite electrodes also increases the fiber reliability. The proposed piezoelectric fibers feature a soft hollow PC core surrounded by a multilayer cladding consisting of the alternating sub-micron-sized piezoelectric/electrode layers, as shown in Figure 1d. PVDF, due to its low cost and availability, is chosen as the principle component in the piezoelectric layers, whereas perovskite ceramic (BTO or PZT) nanoparticles or CNTs are impregnated into PVDF layers in order to enhance their piezoelectric properties. This approach allows replacement of expensive PVDF−TrFE material, while resulting in the comparable or even superior piezoelectric response. The carbon-impregnated low-density polyethylene (C-LDPE) layers serve as electrode layers. By bending or stretching the fibers, piezoelectricity could be effectively generated. Experimentally, a piezoelectric generator using a 10 cm long BTO−PVDF (BTO concentration = 20 wt %) fiber could generate an open-circuit voltage of 1.4 V and a short-circuit current of 0.8 nA when the fiber tip is displaced transversely by 10 mm. The corresponding voltage and current were ∼6 V and ∼4 nA for a PZT−PVDF (20 wt % PZT) fiber generator, and ∼3 V and ∼1.2 nA for a CNT−PVDF (0.4 wt % CNT) fiber generator. Compared to the previous piezoelectric fibers reported,[14,18−21] our fibers adopt a spiral structure and thus have much larger active areas for piezoelectricity generation as well as smaller gaps between the electrodes. As a result, our fibers could generate much higher piezoelectric currents, which are proportional to the number of turns in a spiral. Among other advantages of the piezoelectric fibers reported in this paper are low cost of the materials used in fabrication, light weight, good durability, and the possibility of mass production *via* fiber drawing. As examples of practical applications of the proposed piezoelectric fibers, we present energy-harvesting textiles using BTO−PVDF fibers and characterize their performance in the context of wearable and automotive microgenerators. Moreover, we also present detection of sound using the CNT−PVDF fiber that features piezoelectric voltage generated by sound wave that is proportional to the square root of the acoustic power.

RESULTS AND DISCUSSION

Fabrication of the Piezoelectric Micro/Nanostructured Fibers. Figure 1 summarizes the fabrication process of a piezoelectric fiber. A fiber preform is assembled by co-rolling two PVDF-based piezoelectric mats (thickness = 100 μm) sandwiched between two C-LDPE films (thickness = 85 μm, volume resistivity = 2.2 Ω·m, Bystat International Inc.) around a hollow PC tube (diameter = 25.4 mm, Mcmaster Carr) (Figure 1b,c). Note that the bulk resistivity of conductive

DOI: 10.1021/acsnano.6b08290
ACS Nano XXXX, XXX, XXX−XXX

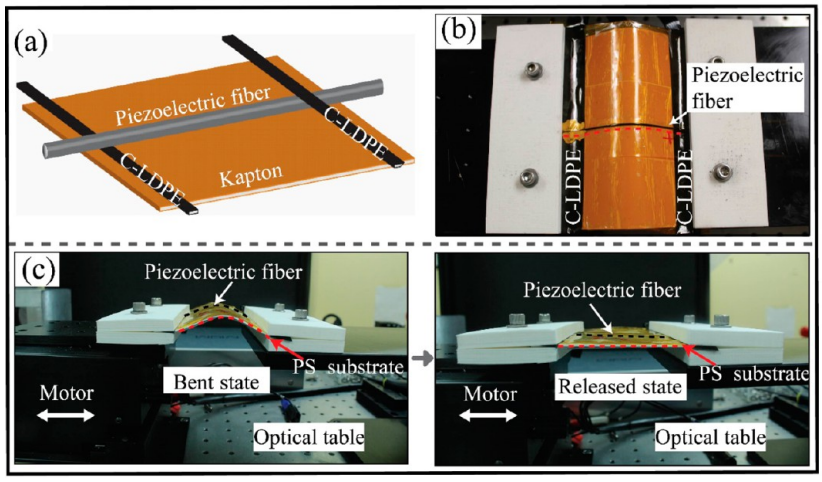

Figure 2. (a) Schematic and a (b) photo of a BTO−PVDF fiber test cell. (c) Fiber in the bent and released states.

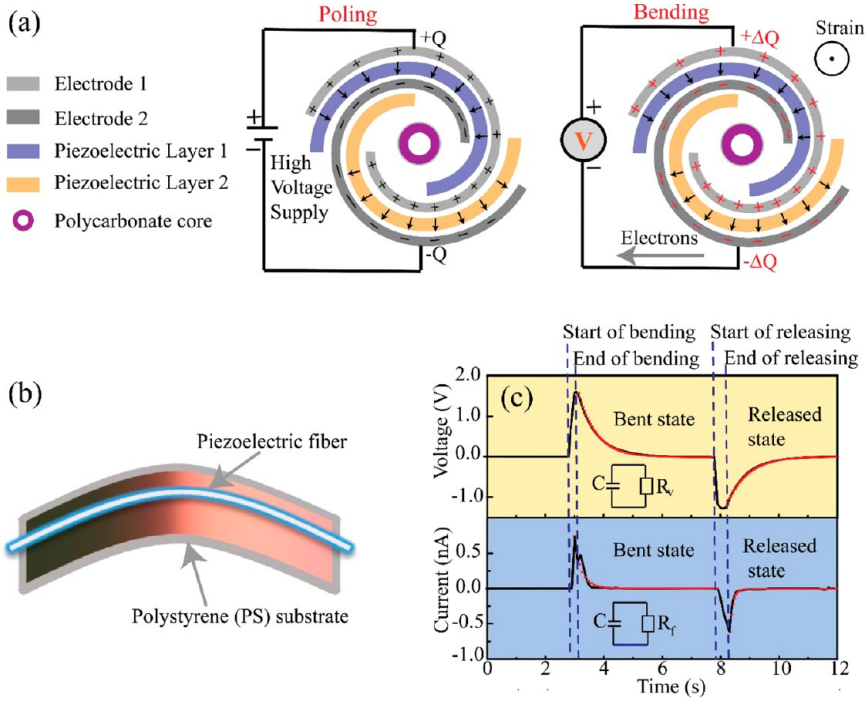

Figure 3. Schematics of the charge separation mechanism in the drawn fibers. (a) All dipoles are oriented in the direction of the local electric fields during electric poling (no bending). When mechanical strain is applied along the device by bending, the polarization density is changed and the electrons are forced to flow from one electrode to the other, thus generating voltage differential. (b) Schematic of a piezoelectric fiber in the bent state. The piezoelectric fiber was attached to a plane PS substrate and covered with Kapton tape in order to induce a uniform strain during bending. (c) Open-circuit voltage and short-circuit current of the piezoelectric fiber during the bend and release actions. The inset image shows the equivalent circuit of the piezoelectric fiber connected to a voltmeter or a current meter. The piezoelectric fiber is modeled as a capacitor C_f; the voltmeter is modeled as a resistor R_v, and the fiber resistance is R_f. The black line represents the measured output signals during the bend and release state. The red squares represent the modeled results during the bend and release state.

polymer layers can change significantly during drawing due to redistribution of the conductive fillers in the polymer matrix. In extreme cases, the conductive polymer layer can even lose its electrical conductivity after drawing. Therefore, care should be taken in the proper choice of drawing parameters. Our measurements suggest that volume resistivity of conductive layers in the drawn fibers are ~2.5 Ω·m. The above-mentioned polymer materials are chosen for fiber fabrication because they have similar processing temperatures, which is important for co-drawing. The conductive layers are spatially offset in order to produce two easily accessible electrodes on the preform surface after rolling the preform. The piezoelectric mats (Figure 1f) used in the preform are BTO−PVDF, PZT−PVDF, or CNT−PVDF nanocomposites, which were fabricated in-house *via* electrospinning. Besides, we also varied the concentrations of BTO and CNT in the mats to study how they would affect the piezoelectric properties of the fabricated fibers. After assembly, the preforms were drawn into piezoelectric fibers using a plastic fiber drawing tower. During fiber drawing, we also explored applications of high voltage (up to 5 kV) to the preform electrodes in order to pole the drawn fibers directly during the fabrication process. We found that while this only

DOI: 10.1021/acsnano.6b08290
ACS Nano XXXX, XXX, XXX−XXX

led to a modest improvement in the piezoelectric functionality of the drawn fibers (since the poling time is insufficient to provide a significant effect), using high voltage we could effectively control the thickness of the layers in the piezoelectric fibers. This is because the conductive electrode layers in a softened preform have a tendency to attract to each other under voltage application, and thus very thin (sub-1 μm) piezoelectric layers could be drawn. In Figure 1d, we show a typical cross section of the piezoelectric fiber (diameter = ~900 μm). The multilayer structure in the fiber cladding was well-maintained during drawing, and thicknesses of the individual piezoelectric or conductive layers typically ranged from 5 to 10 μm. For those fibers drawn under 5 kV, the fiber diameters were reduced to ~300 μm, and thickness of the piezoelectric layers or conductive layers could be less than 1 μm (Figure 1g). Finally, in order to further enhance the fibers' piezoelectric property, they were poled in a silicone oil bath (80 °C) using a voltage of 1 kV for 12 h. The poling voltage was then increased to 5 kV for 12 h and finally to 9 kV for 12 h. The poled fibers were then utilized for development of various piezoelectric generators and energy generation systems.

Characterization of Piezoelectric Micro/Nanostructured Fibers. *Structure of a Test Cell.* In order to characterize fiber piezoelectric properties, we use the following testing method. The two ends of a piezoelectric fiber (length = 10 cm, diameter = ~1 mm) were glued to two C-LDPE strips, as shown in Figure 2a,b. Note that, by design, the fiber features two exposed electrodes positioned on the opposite sides of the fiber surface (see Figure 1c). Thus, before the connection, the piezoelectric fiber should be placed in a specific position: one fiber electrode is on the top, while the other fiber electrode is on the bottom (this can be achieved by rotating the fiber). Then, one C-LDPE strip was attached to the top side of the fiber, while the other one was attached to the bottom side of the fiber on the opposite end. In this way, the two strips would connect to the two different electrodes of the fiber. The piezoelectric fiber together with the C-LDPE strips were immobilized onto a 10 cm long, 1 mm thick PS substrate using Kapton tape. Due to asymmetry in the test cell structure, bending of the PS substrate would lead to a nonzero average strain in the piezoelectric fiber. Experimentally, one end of the PS substrate was fixed, while the other end was horizontally displaced by a micropositioning stage, thus bending the fibers (Figure 2c). The generated voltage and current of the piezoelectric fiber were measured using an Ivium electrochemical workstation (Ivium Technologies).

Charge Separation Mechanism in the Drawn Fibers. As the strain is applied along the microstructured fiber, corresponding positive peaks can be observed in both the output voltage and current measurements. This phenomenon can be explained by examining the charge separation mechanism and equivalent circuit model in Figure 3. During poling, the dipoles of the piezoelectric layers are aligned in the direction of the local electrical fields. After the removal of the poling voltage, the oriented domains maintain a permanent polarization. The electric field of the dipole induces surface charge $+q$ at the top fiber electrode and $-q$ at the bottom fiber electrode. When the fiber is bent, mechanical strain leads to the change of polarization density, which induces change of induced surface charge ($\pm\Delta q$) in the fiber conductive layers.[36,37] In response, the free charges in the fiber electrodes are forced to rebalance this change of charge at a speed set by both the external electric circuit and the built-in potential.[38] In the bent state, the initial increase in the voltage (current) gradually diminishes. Similar to that of piezoelectric film-type generators,[39] this process can be modeled as the RC discharging process with two time constants (τ): a discharging time $\tau_v = R_vC_f$ for open-circuit voltage spike and a discharging time $\tau_c = R_fC_f$ for short-circuit current spike, where C_f is the effective capacitance, R_f is the effective resistance of the piezoelectric fiber, and R_v is the circuit resistance when the fiber is connected to a voltmeter. From Figure 3c, we observe that discharging time for the short-circuit current spike is considerably shorter than discharging time for the open-circuit voltage spike ($\tau_c \sim 0.1$ s $\ll \tau_v \sim 1$ s), thus also signifying that $R_f \ll R_v$. When the strain is removed, the free charges move in the opposite direction, generating a negative voltage (current) spike.

Note that characterization of the electrical properties of the piezoelectric generators is by far not an easy task and deserves a separate paper by itself. The fibers presented in this work have internal structure similar to that of the capacitor fibers detailed in our prior work.[40,41] There, we demonstrated that frequency-dependent electrical properties of the piezoelectric fibers can be modeled using an RC ladder network model. In this model, a fiber is considered as a collection of frequency-dependent transverse and longitudinal resistivities and capacitances, thus resulting in highly nonlinear frequency dependence of the fiber effective complex impedance that cannot be interpreted in terms of simple electrical circuits. Therefore, for the sake of simplicity, in this paper, we resort to qualitative arguments rather than exact derivations. In order to characterize fiber complex impedance, one has to perform an impedance spectroscopy analysis. However, we can approximate the value of the fiber impedance Z_f at low frequencies as a ratio of the open-circuit voltage to the short-circuit current, thus resulting in the values of ~1−2.5 GΩ. Note, however, that this value does not correspond to the resistivity of the in-fiber electrodes but rather represents a value of the complex impedance at a characteristic frequency corresponding to the fiber charge/discharge rate (1−10 Hz; see Figure 3c). At the same time, longitudinal resistance of the in-fiber electrodes, R_f, as well as fiber capacitance, C_f, can be estimated using simple expressions, $R_f \sim \rho\frac{L}{Sd} \sim 2.8$ MΩ and $C_f \sim \frac{\varepsilon_0\varepsilon LS}{d} \sim 46$ nF, where ρ is the bulk resistivity of the in-fiber conductive layers (~2.5 Ω·m), L is the fiber length (~10 cm), S and d are the conductive layer width and thickness, respectively ($S \sim 1.76$ cm; $d \sim 5$ μm), and ε is the dielectric constant of the piezoelectric films ($\varepsilon \sim 15$). Note that the value of R_f can be measured directly as a DC resistivity of a single fiber electrode. From this, we can also estimate a characteristic value for the charge/discharge time constant $\tau_c = R_fC_f \sim 0.1$ s, which is in good agreement with the experimentally measured value (see Figure 3c). At the same time, when the fiber is connected to the voltmeter, the charge/discharge time constant $\tau_v = R_vC_f \sim 1$ s $\gg \tau_c \sim 0.1$ s, which is consistent with the technical information from the voltmeter stating that R_v is in GΩ range. To get a better qualitative comparison with the charge/discharge time constant when the fiber is connected to the voltmeter, one has to consider more carefully the internal structure of the voltmeter and its effective complex impedance. Finally, for more details on the relation between the complex fiber impedance Z_f and the electrode resistivities, fiber capacitance, and frequency, we refer the reader to refs 40 and 41.

DOI: 10.1021/acsnano.6b08290
ACS Nano XXXX, XXX, XXX−XXX

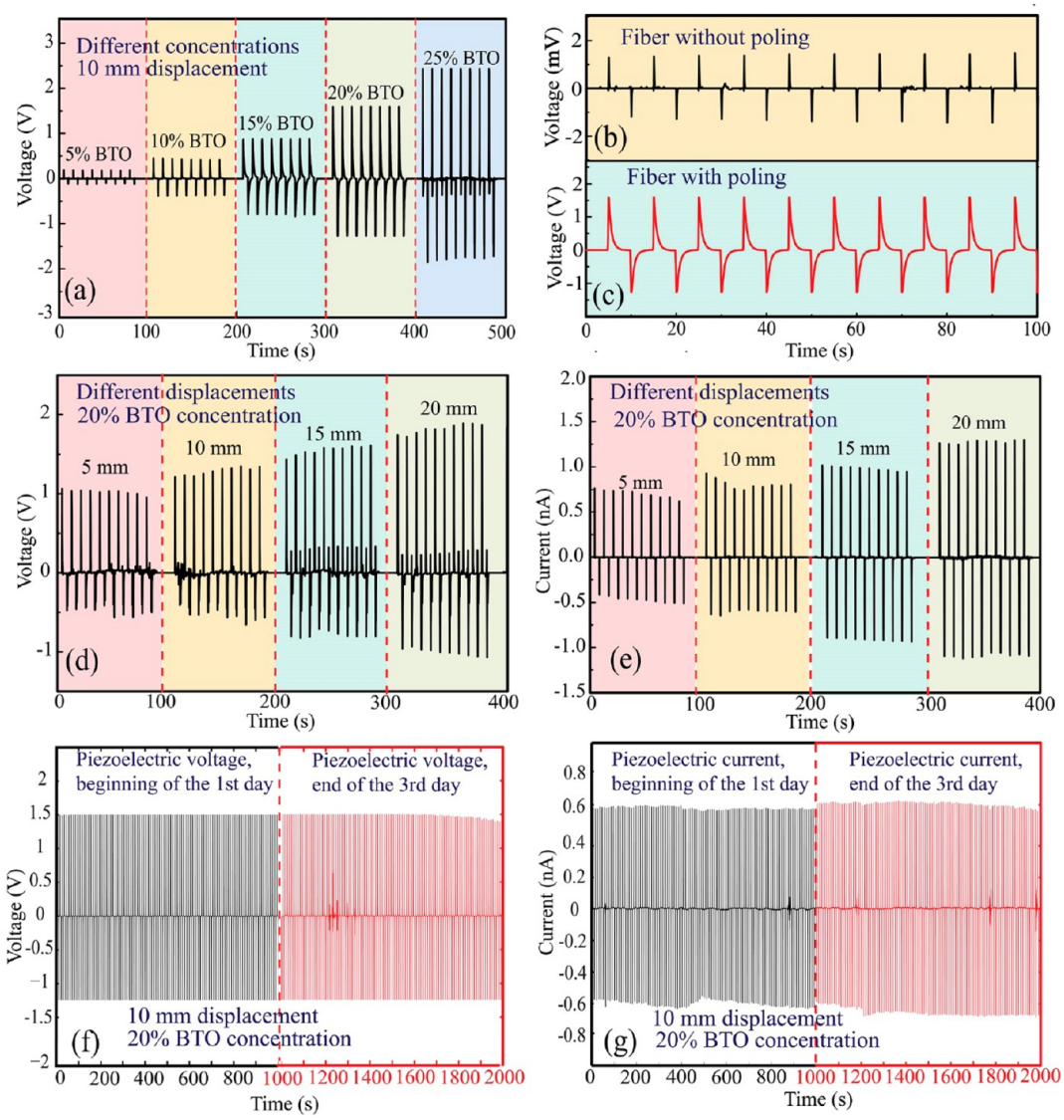

Figure 4. (a) Open-circuit voltage generated by a 10 cm long BTO−PVDF fiber with the BTO concentration of 5, 10, 15, 20, and 25 wt % subjected to a 1 cm displacement. (b,c) Comparison of the piezoelectric voltages generated by the poled BTO−PVDF fiber generator and the unpoled one. (d,e) Open-circuit output voltage and short-circuit current generated by a 10 cm long BTO−PVDF fiber generator (20 wt % BTO in the BTO−PVDF composite) when its moving end is displaced by 5, 10, 15, and 20 mm. (f,g) Durability test for the 10 cm long BTO−PVDF fiber (20 wt % BTO in BTO−PVDF composite) by continuously repeating 1 cm amplitude bend−release movements for 3 days. The open-circuit voltage and short-circuit current generated in a 1000 s period at the beginning of the first day (f) and at the end of the third day (g) are shown.

Characterization of the Piezoelectric Properties of the BTO−PVDF and PZT−PVDF Fibers. We first study the open-circuit voltage generated by the BTO−PVDF fiber generator as a function of the BTO concentration. As the concentration of BTO in the BTO−PVDF layer increased from 5 to 25 wt %, the piezoelectric voltage of a fiber generator with its moving end displaced by 10 mm increased from ∼0.15 to ∼2.5 V (Figure 4a). We find that drawing fibers with BTO concentrations higher than 25 wt % is challenging because at such high BTO concentrations the viscosity of a BTO−PVDF composite is lowered significantly, thus resulting in capillary breakup during fiber drawing. Therefore, to maintain a stable fiber drawing while maximizing piezoelectric functionality, an optimal BTO concentration of 20 wt % was adopted in all of our drawings. In Figure 4d,e, we find that when the moving end of the fiber was displaced by 5−20 mm, the corresponding open-circuit voltage increased from ∼1 to ∼1.7 V, and the short-circuit current increased from ∼0.7 to ∼1.3 nA. Besides, we note that the poling process plays a major role in the functioning of the piezoelectric fibers. The fibers without poling exhibit an open-circuit voltage of ∼1.5 mV, which is 3 orders of magnitude smaller than that of their poled counterparts (Figure 4b,c). A durability test was also conducted for fiber-based generators by continuously repeating the bend−release movements for 3 days. We find that the piezoelectric voltage and current generated by a fiber does not show degradation signs after the entire test that comprises ∼26 000 bend/release cycles (Figure 4f,g).

Next, piezoelectric generators based on PZT−PVDF piezoelectric fibers were studied. The advantage of PZT over BTO is its higher piezoelectric constant. We find that when the moving end of a PZT−PVDF (PZT concentration = 20 wt %) fiber

DOI: 10.1021/acsnano.6b08290
ACS Nano XXXX, XXX, XXX−XXX

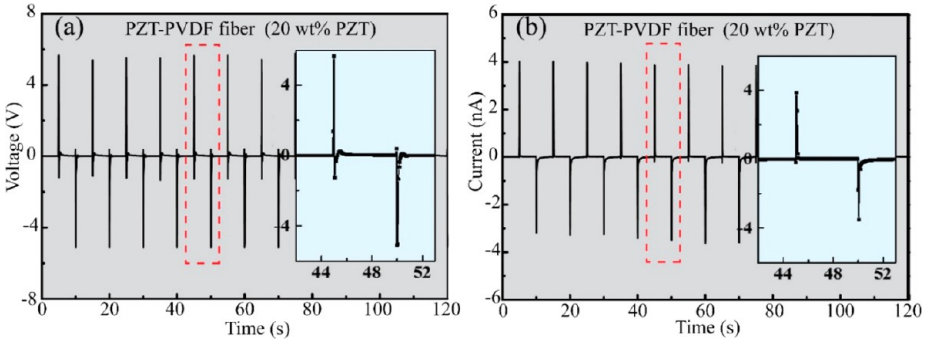

Figure 5. (a,b) Open-circuit voltage and the short-circuit current generated by a 10 cm long PZT−PVDF fiber generator (20 wt % PZT in the PZT−PVDF composite) when its moving end is displaced by 10 mm.

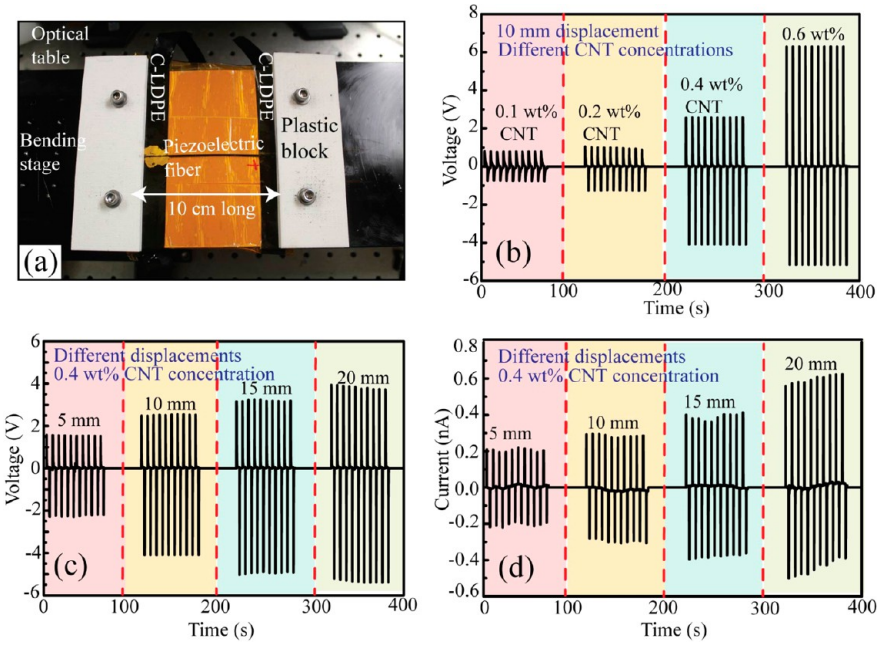

Figure 6. (a) Photo of a CNT/PVDF fiber generator. (b) Open-circuit voltage of a 10 cm long CNT−PVDF fiber generator with CNT concentrations of 0.1, 0.2, 0.4, and 0.6 wt % under 10 mm displacement. (c,d) Open-circuit voltage and short-circuit current of a 10 cm long CNT−PVDF fiber (CNT concentration = 0.4 wt %) when the moving end of the fiber was displaced by 5, 10, 15, and 20 mm.

generator is displaced by 10 mm, it generates an open-circuit voltage of ∼6 V and short-circuit current of ∼4 nA, which are ∼4 times higher than those generated by BTO−PVDF fibers (Figure 5a,b). However, due to the high toxicity of PZT, PZT−PVDF fibers are probably not suitable for wearable applications.

Characterization of the Piezoelectric Properties of the CNT−PVDF Composite Fibers. Piezoelectric generators based on CNT−PVDF fibers were assembled following the same procedures described before. We first studied the dependence of the voltages generated by the CNT−PVDF fibers on CNT concentrations. As shown in Figure 6b, when the moving end of the fiber generators was displaced by 10 mm, the 10 cm long CNT−PVDF fiber generator containing 0.1 wt % CNT generated an open-circuit voltage of ∼0.8 V, while the generator containing 0.6 wt % CNT generated an open-circuit voltage of as high as ∼6.8 V. We, furthermore, find that the fibers with CNT concentrations higher than 0.6 wt % are challenging to fabricate, as they tend to break up during the drawing process. Thus, we adopted an optimal CNT concentration of 0.4 wt % for all of our CNT−PVDF fibers that guaranteed the ease of drawing while maintaining high generated voltage. Figure 6c,d shows that when the moving end of the CNT−PVDF (0.4 wt % CNT) fiber generator was displaced by 5−20 mm, the open-circuit voltage increased from ∼1.7 to ∼3.7 V and the short-circuit current increased from ∼0.2 to ∼0.7 nA. From this, we conclude the performance of the CNT−PVDF (0.4 wt % CNT) fiber generator is comparable to that of the BTO−PVDF (20 wt % BTO) fiber generator.

Examples of Practical Applications of Piezoelectric Fibers. *Stand-Off Distributed Sound Detection.* Our piezoelectric fibers can be used for stand-off sound detection, which opens various possibilities in security and defense applications. In our experiment, the sound wave was generated by a speaker (Dell computer speaker) and software (Adobe Audition CC 2015). Figure 7 shows the structure of the sound wave and the output voltage obtained from the CNT/PVDF fiber (10 cm length). The sound pressure level (SPL) of the actuating sound was ∼20 dB (0.2 mPa) at 1 Hz where dB = 20 $\log_{10}$ (P/P_0), P_0 = 20 μPa, and the amplitude of the fiber output voltage was in the range of 50 to 70 mV. The SPL of the actuating sound was measured using a sound level meter (Larson Davis model 831).

DOI: 10.1021/acsnano.6b08290
ACS Nano XXXX, XXX, XXX−XXX

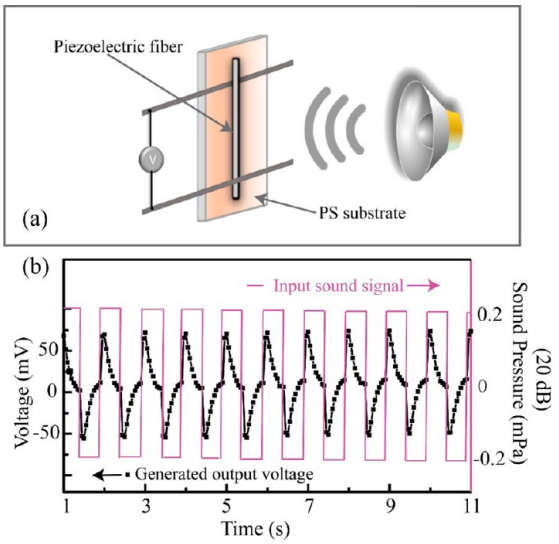

Figure 7. (a) Schematics of the experimental setup. (b) Sound wave (red) and the output voltage from the CNT/PVDF fiber actuated by the sound wave.

When a piezoelectric generator is actuated by the sound waves, the generated voltage V could be generally related to the acoustic power P incident onto the fiber as $V^2 \sim P/f$, where f is the frequency of the applied sound wave, while the time average power incident on the fiber is given by $P = AP_0^2/(2Z_0)$, where P_0 is the local value of the sound wave pressure, A is the fiber surface, and Z_0 is air impedance.[42] Figure 8a shows the output voltage from the CNT/PVDF fiber under the frequencies of 1, 2, 4, 6, 8, and 10 Hz when the input power level of the sound was held constant with the correspondent SPL at ~20 dB. As shown in Figure 8b, the V^2 was linearly dependent on the frequency of the applied sound wave in accordance with ref 42.

Furthermore, we investigate the performance of the sound-driven fiber generator under water. Experimentally, the two ends of a 10 cm long CNT−PVDF fiber were fixed in a water tank with a dimension of 60 cm × 28 cm × 15 cm. An ultrasonic probe was also immersed under water to emit ultrasound waves with a frequency of ~20 kHz. The distance between the probe and the fiber was ~20 cm. While the sonication was repeated with a period of 6 s (1 s on, 5 s off), the piezoelectric voltage generated by the fiber was continuously measured. As the power of the ultrasound wave increased, the amplitude of voltage generated by the CNT−PVDF fiber also increased (Figure 9c,d) according to $V^2 \sim P/f$. We note that in Figure 9c the generated voltage does not return to zero as the off time (5 s) is too short for all the water oscillations in the tank to subside. Normally, the off time should be longer than a minute to see the generation voltage approach a value of zero.

Textile-Based Piezoelectric Generators Woven Using BTO−PVDF Fibers. Here, we present two prototypes of the flexible, textile-based piezoelectric generators. They were fabricated using individual piezoelectric BTO−PVDF fibers and a classic Dobby loom weaving process (Figure 10a,b). We demonstrate that such textile generators could be potentially used as tactile or motion sensors for sports outfits or medical apparel or for micropower generation in automotive and aeronautic industries for powering various electronic devices. In the first prototype, four 20 cm long BTO−PVDF fibers (20 wt % BTO in BTO−PVDF composites) were weaved into a textile and then connected in series. The textile was then tightly wrapped around a human elbow (Figure 10c). In a 90° bend−release action of the elbow, the piezoelectric textile could generate open-circuit voltages of up to ~10 V and short-circuit currents of 5−15 nA (Figure 10d,e).

In the second prototype, fifteen 20 cm long fibers are weaved into a textile and connected in parallel. We then used this textile as a seat pad of a vehicle (Hyundai sedan) and put a 22 kg sandbag on it (Figure 11a). As we drove the vehicle on urban roads, traffic-induced vibration of the vehicle led to distortion of the piezoelectric fibers in the textile, thus generating electric current. A simple full-wave bridge rectifier circuit was used to ensure that the current generated by the

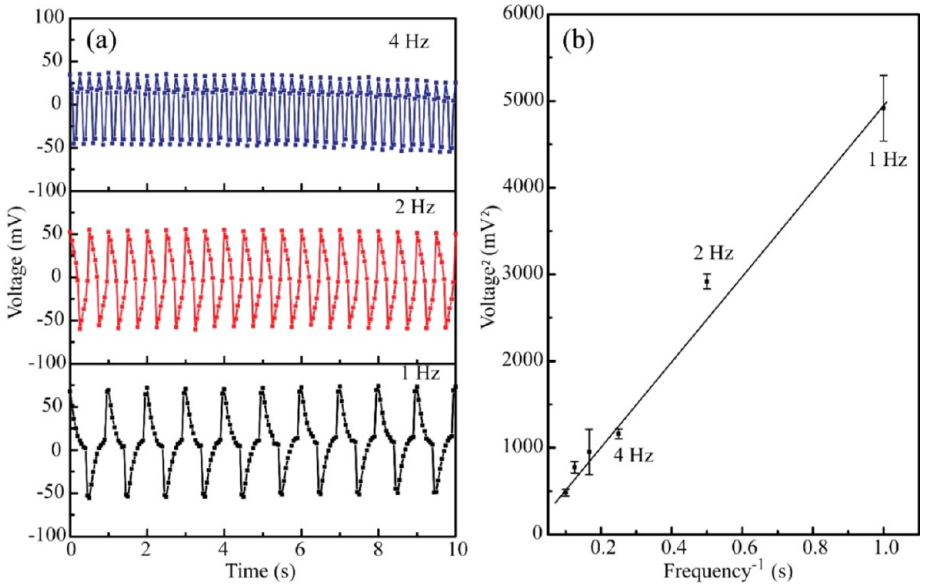

Figure 8. (a) Output voltage generated by the CNT/PVDF fiber at the frequencies of the actuating sound wave of 1, 2, and 4 Hz for SPL of ~20 dB. (b) Output voltage of the piezoelectric fiber *vs* frequency of the sound wave. The error bar is calculated by the standard deviation of the peak value of measured pulses.

DOI: 10.1021/acsnano.6b08290
ACS Nano XXXX, XXX, XXX−XXX

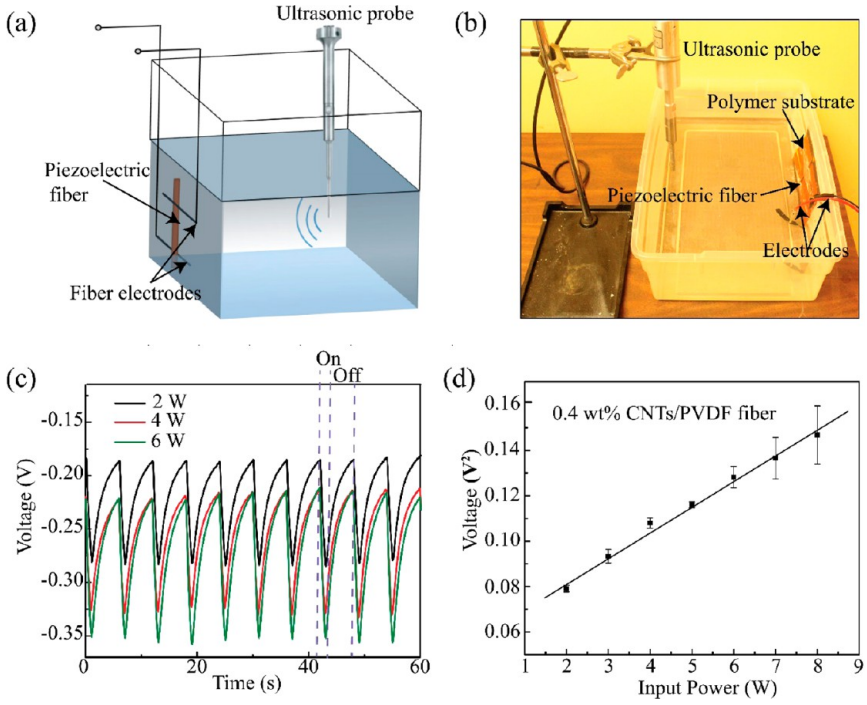

Figure 9. (a) Schematic and a (b) photo of the experimental setup of the underwater ultrasound detection using a CNT−PVDF fiber. (c) Piezoelectric voltages generated by the fiber when the source acoustic powers were 2, 4, and 6 W. (d) Square of the piezoelectric voltage generated by the generator has a linear relation with the acoustic power. The error bar is calculated by the standard deviation of the peak value of measured pulses.

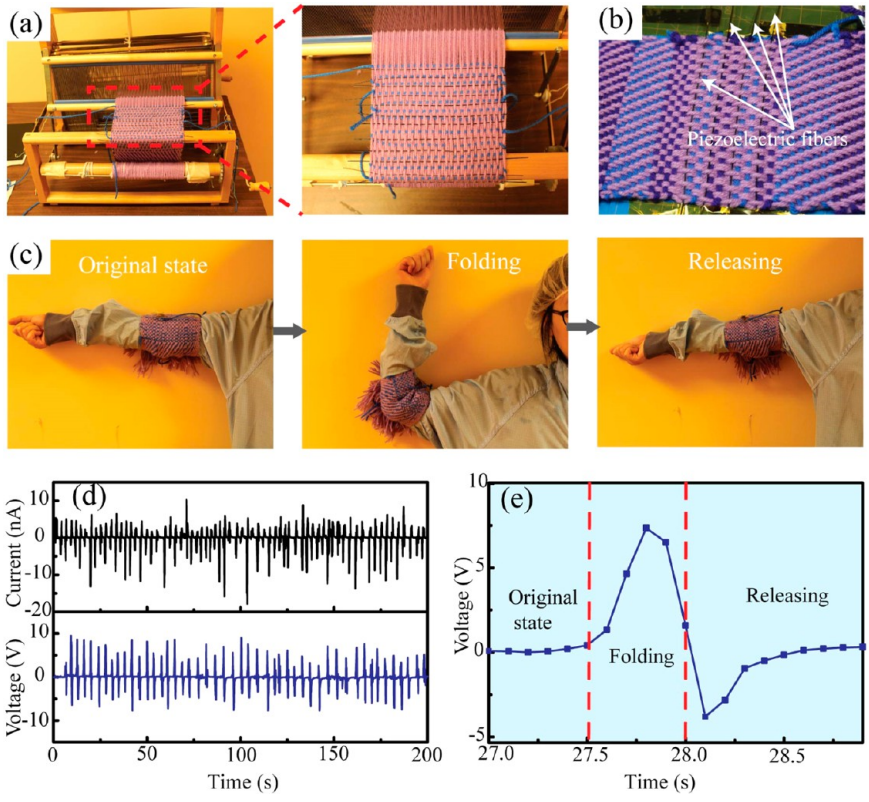

Figure 10. (a) Dobby loom was used to weave piezoelectric fibers into a cotton textile. During weaving, cotton yarns are used as a warp (longitudinal threads forming the textile base). Piezoelectric fibers are introduced during weaving as a weft by passing them through the warp cotton yarns. (b) Cotton-based textile containing four piezoelectric fibers woven using a Dobby loom. (c) Electrical properties of the piezoelectric textile in a 90° folding−release action of the elbow. (d) Open-circuit voltages and short-circuit currents generated by the piezoelectric textile during repeated fold−release motion of the elbow. (e) Open-circuit voltage of the piezoelectric textile in a fold−release elbow action.

DOI: 10.1021/acsnano.6b08290
ACS Nano XXXX, XXX, XXX−XXX

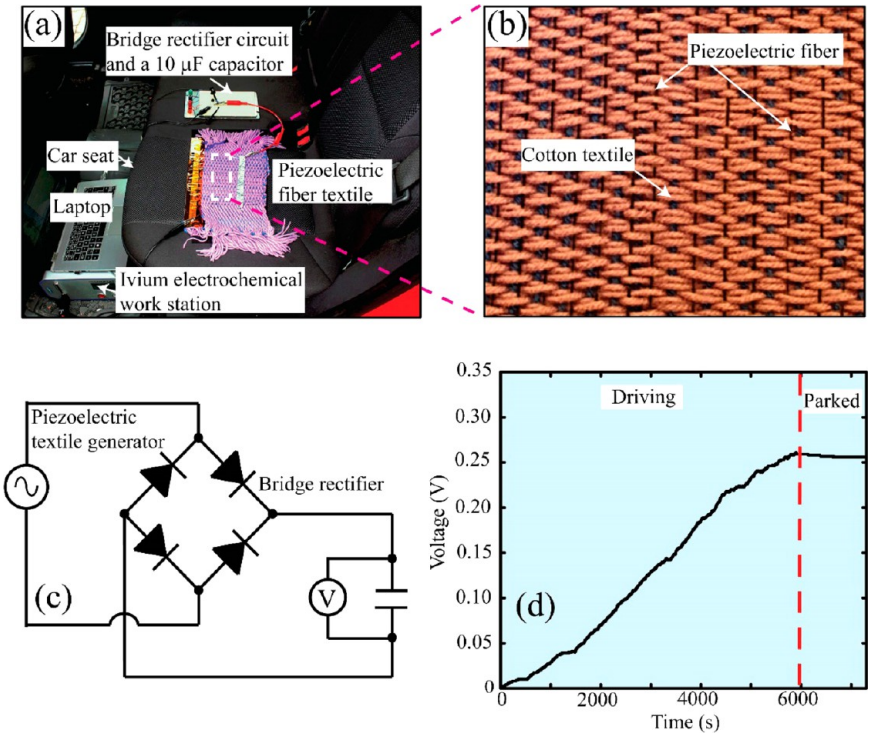

Figure 11. (a) Photo of the experimental setup for the in-car test. The piezoelectric fiber textile (b) (consisting of fifteen 20 cm long piezoelectric fibers connected in parallel) was utilized as an automotive microgenerator pad to charge a 10 μF capacitor *via* a bridge rectifier circuit shown in (c). (d) Voltage of the capacitor charged by a piezoelectric textile during driving and stationary state of the vehicle.

textiles would charge a 10 μF capacitor with consistent polarity (Figure 11c). During a 6000 s period of urban road driving under regular traffic conditions, the piezoelectric textile was able to charge the capacitor from 0 to ~0.3 V (Figure 11d). The charging rate could be further improved by adding more fibers to the power generation pad.

CONCLUSIONS

In summary, we have studied several material combinations, piezoelectric fiber designs, and manufacturing techniques that allow fabrication of piezoelectric fibers with greatly enhanced piezoelectric properties compared to the existing counterparts. The micro/nanostructured piezoelectric fibers presented here feature a soft hollow PC core surrounded by a multilayer cladding consisting of alternating PVDF-based nanocomposite layers and conductive (C-LDPE) layers. We have also performed a comparative study of three material combinations. A BTO/PVDF microstructured fiber (10 cm long; BTO concentration = 20 wt %) could generate an open-circuit voltage of 1.4 V and a short-circuit current of 0.8 nA when the moving end of the generator was displaced transversely by 10 mm. The corresponding voltage and current were ~6 V and ~4 nA for a PZT−PVDF (20 wt % PZT) fiber generator and ~3 V and ~1.2 nA for a CNT−PVDF (0.4 wt % CNT) fiber generator. Perovskite ceramics (such as BTO and PZT) could improve the fiber performance owing to their high piezoelectric coefficient. On the other hand, CNT could induce the crystallization of a polar phase in PVDF layers, thus leading to remarkable improvements in piezoelectric performance. Also we note in passing that the CNT/PVDF microstructured fibers are easier to draw to smaller diameters and they appear to have better mechanical flexibility. The resultant fibers exhibit excellent durability with high piezoelectric voltages (of up to 6 V) in a cyclic bend−release test (greater than 26 000 cycles). Finally, we have presented several examples of the practical applications of the proposed piezoelectric fibers: for a distributed stand-off sound detector using CNT−PVDF fibers and for energy harvesting using textile-based piezoelectric generators that incorporate BTO−PVDF fibers.

The microstructured fibers developed in this work have the following advantages compared to other existing piezoelectric fibers. First, the proposed piezoelectric fibers adopt a spiral multilayer structure, which considerably increases the active areas of the piezoelectric materials and thus results in higher energy generation efficiency. The piezoelectric performance of the proposed fibers could be further improved simply by increasing the number of piezoelectric layers in the fiber structure. Second, the outermost C-LDPE layers serve as two spatially offset electrodes on the fiber surface, thus greatly simplifying connectorization to our fibers. Third, owing to the thermal fiber drawing process, the dimensions of piezoelectric fibers can be as small as hundreds of microns, which enables their applications inside small tubes, such as blood vessels.[25,43,44] Moreover, the soft piezoelectric fibers with well-controlled geometries can be woven into low-cost fabrics that allow wearable, portable, and large-area applications. Other advantages include use of low-cost materials during fabrication, high flexibility, good durability, and possibility of mass production using a fiber drawing technique.

EXPERIMENTAL SECTION

Solution Preparation. *BTO−PVDF Solution Preparation.* BTO (nanoparticles with average diameter of 200 nm; US Research Nanomaterials Inc.) of defined amount was dispersed in dimethylformamide (DMF) solvent (Sigma-Aldrich) using a probe-type sonicator (Fisher Scientific Inc.) at 100 W in 5 s intervals (3 s pulse on, 2 s pulse off) for 1 h. PVDF (pellet, M_w ~ 275 000, Sigma-Aldrich) was

DOI: 10.1021/acsnano.6b08290
ACS Nano XXXX, XXX, XXX−XXX

dispersed in acetone using a magnetic stirrer for 10 min. Then, the BTO solution and the PVDF solution were mixed together while being heated at 100 °C using a magnetic stirrer for 1 h. Subsequently, the BTO−PVDF solution was sonicated at 75 W in 5 s intervals (3 s pulse on, 2 s pulse off) for 15 min and then put in a vacuum chamber for 5 min to remove air bubbles. In our experiments, the concentration of PVDF in the solution was 20 wt %, and weight concentration of BTO in the as-spun BTO−PVDF composite mats was varied from 5 to 25 wt % with a 5 wt % interval. The DMF/acetone volume ratio was 2/3.

PZT−PVDF Solution Preparation. PZT powders (APC 850) purchased from APC Inc. generally have a size ranging from 10 to 50 μm. To reduce the PZT particle size and thus enhance their piezoelectric functionality, PZT powders were milled using a ball-milling machine (MSK-SFM-2, MTI Corporation) for 10 h with a milling speed of 200 rpm. Ten ZrO_2 balls with a diameter of 10 mm were used as the milling medium. The weight ratio of PZT powders to the milling balls was 1:20. The milled PZT powders could be then used for the preparation of PZT−PVDF solutions, which follows exactly the same procedures as used for BTO−PVDF solutions.

CNT−PVDF Solution Preparation. Multiwalled carbon nanotubes (Sigma-Aldrich) of defined amount were dispersed in DMF solvent using an ultrasonicator for 15 min. PVDF (pellet, $M_w \sim 275\,000$, Sigma-Aldrich) was dispersed in acetone using a magnetic stirrer for 10 min. Then, the CNT solution and the PVDF solution were mixed together while being heated at 100 °C using a magnetic stirrer for 1 h. Subsequently, the CNT−PVDF solution was sonicated at 75 W in 5 s intervals (3 s pulse on, 2 s pulse off) for 15 min and then put in a vacuum chamber for 5 min to remove air bubbles. In our experiments, the concentration of PVDF in the solution was 20 wt %, and the weight concentration of the CNT in the as-spun BTO−PVDF composite mats was varied from 0.2, 0.4, and 0.6 wt %. The DMF/acetone volume ratio was 2/3.

Electrospinning of BTO−PVDF, PZT−PVDF, and CNT−PVDF Solutions. The as-prepared PVDF-based composite (BTO−PVDF, PZT−PVDF, or CNT−PVDF) solutions were electrospun using an electrospinning workstation (MSK-NFES-3, MTI Corporation) to fabricate the corresponding mats. In electrospinning, the solution was first loaded into a glass syringe (Hamilton, 20 mL) equipped with a blunt metallic needle (Hamilton, 22 gauge). A high voltage of 15 kV was then applied to the syringe needle, while a drum collector (diameter = 5 cm) used as the substrate of the as-electrospun mat was grounded. The distance between the needle tip and the drum collector was ∼15 cm. The spinning solution was delivered to the needle tip at a flow rate of 1 mL·h^{-1}. To ensure uniformity of the thickness of the electrospun mat, the syringe was mounted onto a motor-driven platform that scans tangentially to the drum collector with a speed of 2 mm/s. A scanning electron microscopy image of the as-electrospun BTO−PVDF mats is shown in Figure 1f.

Preparation of the Piezoelectric Fiber Preforms and Fiber Drawing. To fabricate the fiber preform, four alternating PVDF-based composite mats (100 μm thick) and C-LDPE films (85 μm thick) are co-rolled around a hollow PC tube, as shown in Figure 1b. Before drawing, the preform was consolidated in a vacuum furnace at 110 °C for ∼24 h. The preform was then drawn at 190 °C into piezoelectric fibers using the fiber drawing technique. In particular, the preform was placed into the vertical furnace of the fiber drawing tower, where the temperature is increased above the polymer softening temperature. As a consequence, the preform tip melts and forms a blob that later falls down under the force of gravity, thus creating a slender fiber that can be continuously pulled from the molten preform tip. In actuality, a clamp tractor is used to continuously pull the fiber at a constant speed. The final size of a resultant fiber depends on the parameters used in the drawing process such as fiber drawing speed, temperature distribution in the furnace, preform feeding speed, as well as overpressure used during fiber fabrication. Experimentally, we set the drawing speed as 500 mm/min and used an air pressure of 3 mbar to pressurize the fiber core during drawing.

Electrical Measurements. The open-circuit voltage and short-circuit current of the devices were measured by an electrochemical station (Ivium Technologies). The sampling time constant was 0.1 s. The bend/release actions of the devices were controlled by a micropositioning stage. The displacement velocity during bend/release cycles was 5 cm/s. The bend/release cycle was repeated every 10.4 s. During each cycle, the bend motion lasted 0.2 s, followed by a pause of 5 s in the bent state, followed by 0.2 s of the release motion, and finally followed by a 5 s pause in the released state.

ASSOCIATED CONTENT

Supporting Information

The Supporting Information is available free of charge on the ACS Publications website at DOI: 10.1021/acsnano.6b08290.

More details of the effects of the fiber length on the output voltage and current of the piezoelectric devices (PDF)

AUTHOR INFORMATION

Corresponding Author

*E-mail: maksim.skorobogatiy@polymtl.ca.

ORCID

Xin Lu: 0000-0002-8792-3750

Notes

The authors declare no competing financial interest.

ACKNOWLEDGMENTS

We thank Natural Science and Engineering Research Council of Canada for their support of this work *via* a STPGP447326-13 strategic grant. We thank also NanoQuébec for their support *via* Grant Rg-006 with the contribution of Airbus Defence and Space. Finally, we thank China Scholarship Council for the student support.

REFERENCES

(1) Caliò, R.; Rongala, U. B.; Camboni, D.; Milazzo, M.; Stefanini, C.; de Petris, G.; Oddo, C. M. Piezoelectric Energy Harvesting Solutions. *Sensors* **2014**, *14*, 4755−4790.

(2) Siddique, A. R. M.; Mahmud, S.; Van Heyst, B. A Comprehensive Review on Vibration Based Micro Power Generators Using Electromagnetic and Piezoelectric Transducer Mechanisms. *Energy Convers. Manage.* **2015**, *106*, 728−747.

(3) Mishra, R.; Jain, S.; Prasad, C. D. A Review on Piezoelectric Material as a Source of Generating Electricity and Its Possibility to Fabricate Devices for Daily Uses of Army Personnel. *Int. J. Syst. Contr. Comm* **2015**, *6*, 212−221.

(4) Ramadan, K. S.; Sameoto, D.; Evoy, S. A Review of Piezoelectric Polymers as Functional Materials for Electromechanical Transducers. *Smart Mater. Struct.* **2014**, *23*, 033001.

(5) Ramli, M. H. M.; Yunus, M. H. M.; Low, C. Y.; Jaffar, A. Scavenging Energy from Human Activities Using Piezoelectric Material. *Procedia Technology* **2014**, *15*, 827−831.

(6) M'boungui, G.; Adendorff, K.; Naidoo, R.; Jimoh, A. A.; Okojie, D. E. A Hybrid Piezoelectric Micro-Power Generator for Use in Low Power Applications. *Renewable Sustainable Energy Rev.* **2015**, *49*, 1136−1144.

(7) Anand, S.; Soin, N.; Shah, T.; Siores, E. Energy Harvesting "3-D Knitted Spacer" Based Piezoelectric Textiles. *IOP Conf. Ser.: Mater. Sci. Eng.* **2016**, *141*, 012001.

(8) Kim, K. Biocompatible and Flexible Nanogenerators for Wearable and Implantable Mechano-Energy Harvester. M.S. Thesis, Ulsan National Institute of Science and Technology, South Korea, 2015.

(9) Tao, X. *Wearable Electronics and Photonics*; Woodhead Publishing: Cambridge, U.K., 2005; pp 1−12.

(10) Lee, J.; Choi, B. Development of a Piezoelectric Energy Harvesting System for Implementing Wireless Sensors on the Tires. *Energy Convers. Manage.* **2014**, *78*, 32−38.

DOI: 10.1021/acsnano.6b08290
ACS Nano XXXX, XXX, XXX−XXX

(11) Mouapi, A.; Hakem, N.; Delisle, G. Y.; Kandil, N. A Novel Piezoelectric Micro-Generator to Power Wireless Sensors Networks in Vehicles, *IEEE International Conference on Environment and Electrical Engineering (EEEIC)*, Rome, Italy, June 10−13, 2015.
(12) Zeng, W.; Tao, X. M.; Chen, S.; Shang, S.; Chan, H. L. W.; Choy, S. H. Highly Durable All-Fiber Nanogenerator for Mechanical Energy Harvesting. *Energy Environ. Sci.* **2013**, *6*, 2631−2638.
(13) Qiu, J.; Tani, J.; Yamada, N.; Takahashi, H. Fabrication of Piezoelectric Fibers with Metal Core. *Proc. SPIE* **2003**, *5053*, 475−483.
(14) Qin, Y.; Wang, X.; Wang, Z. L. Microfibre−Nanowire Hybrid Structure for Energy Scavenging. *Nature* **2008**, *451*, 809−813.
(15) Lee, M.; Chen, C. Y.; Wang, S.; Cha, S. N.; Park, Y. J.; Kim, J. M.; Chou, L. J.; Wang, Z. L. A Hybrid Piezoelectric Structure for Wearable Nanogenerators. *Adv. Mater.* **2012**, *24*, 1759−1764.
(16) Zhang, L.; Bai, S.; Su, C.; Zheng, Y.; Qin, Y.; Xu, C.; Wang, Z. L. A High-Reliability Kevlar Fiber-ZnO Nanowires Hybrid Nanogenerator and Its Application on Self-Powered UV Detection. *Adv. Funct. Mater.* **2015**, *25*, 5794−5798.
(17) Wang, R.; Xin, J. H.; Tao, X. M.; Daoud, W. A. ZnO Nanorods Grown on Cotton Fabrics at Low Temperature. *Chem. Phys. Lett.* **2004**, *398*, 250−255.
(18) Lund, A.; Hagström, B. Melt Spinning of β-Phase Poly(vinylidene fluoride) Yarns with and without a Conductive Core. *J. Appl. Polym. Sci.* **2011**, *120*, 1080−1089.
(19) Lund, A.; Jonasson, C.; Johansson, C.; Haagensen, D.; Hagström, B. Piezoelectric Polymeric Bicomponent Fibers Produced by Melt Spinning. *J. Appl. Polym. Sci.* **2012**, *126*, 490−500.
(20) Glauß, B.; Steinmann, W.; Walter, S.; Beckers, M.; Seide, G.; Gries, T.; Roth, G. Spinnability and Characteristics of Polyvinylidene Fluoride (PVDF)-Based Bicomponent Fibers with a Carbon Nanotube (CNT) Modified Polypropylene Core for Piezoelectric Applications. *Materials* **2013**, *6*, 2642−2661.
(21) Liu, W.; Chen, R.; Ruan, X.; Fu, X. Polymeric Piezoelectric Fiber with Metal Core Produced by Electrowetting-Aided Dry Spinning Method. *J. Appl. Polym. Sci.* **2016**, *133*, 43968.
(22) Soin, N.; Shah, T. H.; Anand, S. C.; Geng, J.; Pornwannachai, W.; Mandal, P.; Reid, D.; Sharma, S.; Hadimani, R. L.; Bayramol, D. V.; et al. Novel "3-D Spacer" All Fibre Piezoelectric Textiles for Energy Harvesting Applications. *Energy Environ. Sci.* **2014**, *7*, 1670−1679.
(23) Yetisen, A. K.; Qu, H.; Manbachi, A.; Butt, H.; Dokmeci, M. R.; Hinestroza, J. P.; Skorobogatiy, M.; Khademhosseini, A.; Yun, S. H. Nanotechnology in Textiles. *ACS Nano* **2016**, *10*, 3042−3068.
(24) *Electronic Textiles: Smart Fabrics and Wearable Technology*; Dias, T., Ed.; Woodhead Publishing: Cambridge, U.K., 2015.
(25) Egusa, S.; Wang, Z.; Chocat, N.; Ruff, Z. M.; Stolyarov, A. M.; Shemuly, D.; Sorin, F.; Rakich, P. T.; Joannopoulos, J. D.; Fink, Y. Multimaterial Piezoelectric Fibres. *Nat. Mater.* **2010**, *9*, 643−648.
(26) Kanik, M.; Aktas, O.; Sen, H. S.; Durgun, E.; Bayindir, M. Spontaneous High Piezoelectricity in Poly(vinylidene fluoride) Nanoribbons Produced by Iterative Thermal Size Reduction Technique. *ACS Nano* **2014**, *8*, 9311−9323.
(27) Hao, Y.; Wang, X.; O'Brien, S.; Lombardi, J.; Li, L. Flexible $BaTiO_3$/PVDF Gradated Multilayer Nanocomposite Film with Enhanced Dielectric Strength and High Energy Density. *J. Mater. Chem. C* **2015**, *3*, 9740−9747.
(28) Zhao, Y.; Liao, Q.; Zhang, G.; Zhang, Z.; Liang, Q.; Liao, X.; Zhang, Y. High Output Piezoelectric Nanocomposite Generators Composed of Oriented $BaTiO_3$ NPs@PVDF. *Nano Energy* **2015**, *11*, 719−727.
(29) Vatansever, D.; Hadimani, R.; Shah, T.; Siores, E. An Investigation of Energy Harvesting from Renewable Sources with PVDF and PZT. *Smart Mater. Struct.* **2011**, *20*, 055019.
(30) Ahn, Y.; Lim, J. Y.; Hong, S. M.; Lee, J.; Ha, J.; Choi, H. J.; Seo, Y. Enhanced Piezoelectric Properties of Electrospun Poly(vinylidene fluoride)/Multiwalled Carbon Nanotube Composites Due to High β-Phase Formation in Poly(vinylidene fluoride). *J. Phys. Chem. C* **2013**, *117*, 11791−11799.
(31) Huang, S.; Yee, W. A.; Tjiu, W. C.; Liu, Y.; Kotaki, M.; Boey, Y. C. F.; Ma, J.; Liu, T.; Lu, X. Electrospinning of Polyvinylidene Difluoride with Carbon Nanotubes: Synergistic Effects of Extensional Force and Interfacial Interaction on Crystalline Structures. *Langmuir* **2008**, *24*, 13621−13626.
(32) Rath, S. K.; Dubey, S.; Kumar, G. S.; Kumar, S.; Patra, A.; Bahadur, J.; Singh, A.; Harikrishnan, G.; Patro, T. U. Multi-Walled CNT-Induced Phase Behaviour of Poly(vinylidene fluoride) and Its Electro-Mechanical Properties. *J. Mater. Sci.* **2014**, *49*, 103−113.
(33) Mago, G.; Fisher, F. T.; Kalyon, D. M. Deformation-Induced Crystallization and Associated Morphology Development of Carbon Nanotube-PVDF Nanocomposites. *J. Nanosci. Nanotechnol.* **2009**, *9*, 3330−3340.
(34) Wu, C. M.; Chou, M. H. Polymorphism, Piezoelectricity and Sound Absorption of Electrospun PVDF Membranes with and without Carbon Nanotubes. *Compos. Sci. Technol.* **2016**, *127*, 127−133.
(35) Yee, W. A.; Kong, J. H.; Zhang, C.; Liu, T. X.; Kotaki, M.; Lu, X. H. Polymorphism of Electrospun Polyvinylidene Difluoride/Carbon Nanotube (CNT) Nanocomposites: Synergistic Effects of CNT Surface Chemistry, Extensional Force and Supercritical Carbon Dioxide Treatment. *Polymer* **2012**, *53*, 5097−5102.
(36) Katsouras, I.; Asadi, K.; Li, M.; van Driel, T. B.; Kjaer, K. S.; Zhao, D.; Lenz, T.; Gu, Y.; Blom, P. W. M.; Damjanovic, D.; et al. The Negative Piezoelectric Effect of the Ferroelectric Polymer Poly(vinylidene fluoride). *Nat. Mater.* **2016**, *15*, 78−84.
(37) Furukawa, T.; Wen, J. X.; Suzuki, K.; Takashina, Y.; Date, M. Piezoelectricity and Pyroelectricity in Vvinylidene Fluoride/Trifluoroethylene Vopolymers. *J. Appl. Phys.* **1984**, *56*, 829−834.
(38) Chang, C.; Tran, V. H.; Wang, J.; Fuh, Y. K.; Lin, L. Direct-Write Piezoelectric Polymeric Nanogenerator with High Energy Conversion Efficiency. *Nano Lett.* **2010**, *10*, 726−731.
(39) Park, K. I.; Lee, M.; Liu, Y.; Moon, S.; Hwang, G. T.; Zhu, G.; Kim, J. E.; Kim, S. O.; Kim, D. K.; Wang, Z. L.; et al. Flexible Nanocomposite Generator Made of $BaTiO_3$ Nanoparticles and Graphitic Carbons. *Adv. Mater.* **2012**, *24*, 2999−3004.
(40) Gu, J. F.; Gorgutsa, S.; Skorobogatiy, M. Soft Capacitor Fibers Using Conductive Polymers for Electronic Textiles. *Smart Mater. Struct.* **2010**, *19*, 115006.
(41) Gorgutsa, S.; Gu, J. F.; Skorobogatiy, M. A Woven 2D Touchpad Sensor and a 1D Slide Sensor Using Soft Capacitor Fibers. *Smart Mater. Struct.* **2012**, *21*, 015010.
(42) Cha, S. N.; Seo, J. S.; Kim, S. M.; Kim, H. J.; Park, Y. J.; Kim, S. W.; Kim, J. M. Sound-Driven Piezoelectric Nanowire-Based Nanogenerators. *Adv. Mater.* **2010**, *22*, 4726−4730.
(43) Zhou, Q.; Lam, K. H.; Zheng, H.; Qiu, W.; Shung, K. K. Piezoelectric Single Crystal Ultrasonic Transducers for Biomedical Applications. *Prog. Mater. Sci.* **2014**, *66*, 87−111.
(44) Kolkman, R. G. M.; Hondebrink, E.; Steenbergen, W.; de Mul, F. F. M. *In Vivo* Photoacoustic Imaging of Blood Vessels Using an Extreme-Narrow Aperture Sensor. *IEEE J. Sel. Top. Quantum Electron.* **2003**, *9*, 343−346.

DOI: 10.1021/acsnano.6b08290
ACS Nano XXXX, XXX, XXX−XXX